

1 A versatile platform strain for high-fidelity multiplex genome editing

2 Robert G. Egbert^{1,†}, Harneet S. Rishi^{2,3,†}, Benjamin A. Adler^{4,5}, Dylan M. McCormick⁵, Esteban Toro⁵,
3 Ryan T. Gill⁶ and Adam P. Arkin^{1,5,*}

4 ¹ Environmental Genomics and Systems Biology Division, Lawrence Berkeley National Laboratory,
5 Berkeley, CA, 94720, USA

6 ² Biophysics Graduate Group, University of California - Berkeley, Berkeley, CA, 94720, USA

7 ³ Designated Emphasis Program in Computational and Genomic Biology, University of California -
8 Berkeley, Berkeley, CA, 94720, USA

9 ⁴ UC Berkeley-UCSF Graduate Program in Bioengineering, University of California - Berkeley,
10 Berkeley, CA, 94720, USA

11 ⁵ Department of Bioengineering, University of California - Berkeley, Berkeley, CA, 94720, USA

12 ⁶ Department of Chemical and Biomolecular Engineering, University of Colorado Boulder, Boulder,
13 CO, 80309, USA

14 [†] The authors wish it to be known that, in their opinion, the first two authors should be regarded as
15 joint First Authors.

16 * To whom correspondence should be addressed. Tel: 510-495-2366; Fax: 510-486-6219; Email:
17 aparkin@lbl.gov.

18 Present Address: Robert G. Egbert, Biological Sciences Division, Pacific Northwest National
19 Laboratory, Richland, WA 99354, USA.

20

21 ABSTRACT

22 Precision genome editing accelerates the discovery of the genetic determinants of phenotype and the
23 engineering of novel behaviors in organisms. Advances in DNA synthesis and recombineering have
24 enabled high-throughput engineering of genetic circuits and biosynthetic pathways via directed
25 mutagenesis of bacterial chromosomes. However, the highest recombination efficiencies have to date
26 been reported in persistent mutator strains, which suffer from reduced genomic fidelity. The absence of
27 inducible transcriptional regulators in these strains also prevents concurrent control of genome
28 engineering tools and engineered functions. Here, we introduce a new recombineering platform strain,
29 BioDesignER, which incorporates (1) a refactored λ -Red recombination system that reduces toxicity
30 and accelerates multi-cycle recombination, (2) genetic modifications that boost recombination
31 efficiency, and (3) four independent inducible regulators to control engineered functions. These
32 modifications resulted in single-cycle recombineering efficiencies of up to 25% with a seven-fold
33 increase in recombineering fidelity compared to the widely used recombineering strain EcNR2. To
34 facilitate genome engineering in BioDesignER, we have curated eight context-neutral genomic loci,
35 termed Safe Sites, for stable gene expression and consistent recombination efficiency. BioDesignER is
36 a platform to develop and optimize engineered cellular functions and can serve as a model to implement
37 comparable recombination and regulatory systems in other bacteria.

38 INTRODUCTION

39 The design-build-test (DBT) cycle is a common paradigm used in engineering disciplines. Within the
40 context of synthetic biology it is employed to engineer user-defined cellular functions for applications

41 such as metabolic engineering, biosensing, and therapeutics (1, 2). The rapid prototyping of engineered
42 functions has been facilitated by advances in *in vitro* DNA assembly, and plasmids have traditionally
43 been used to implement designs *in vivo* given their ease-of-assembly and portability. However, for
44 deployment in contexts beyond the laboratory such as large-scale industrial bioprocesses or among
45 complex microbial communities, plasmid-based circuits suffer from multiple limitations: high intercellular
46 variation in gene expression, genetic instability from random partitioning of plasmids during cell division,
47 and plasmid loss in environments for which antibiotic use could disrupt native microbial communities or
48 is economically infeasible (3, 4). These shortcomings can be ameliorated once a design is transferred
49 from a plasmid to the host genome, which offers improved genetic stability and lower expression
50 variation (5) along with reduced metabolic load (6). However, behaviors optimized for plasmid contexts
51 often do not map predictably to the genome. As such, building and testing designs directly on the
52 genome can reduce the DBT cycle time and facilitate engineering cellular programs for complex
53 environments.

54

55 Expanding synthetic biology efforts to genome-scale engineering has historically been limited by factors
56 such as low endogenous rates of recombination, lack of optimized workflows for recombination, and
57 uncertainty due to locus-dependent expression variability (7, 8). The advent of recombination-based
58 genetic engineering (recombineering), which relies on homologous recombination proteins, often *exo*,
59 *bet*, and *gam* from bacteriophage λ , in conjunction with linear donor DNA containing target homology
60 and the desired mutations, has enabled genomic deletions, insertions, and point mutations at user-
61 defined loci (9-13). Recombineering has enabled generation of genomic discovery resources such as
62 the *E. coli* K-12 in-frame, single-gene deletion collection of non-essential genes (Keio collection) (14)
63 and technologies such as trackable multiplex recombineering (TRMR), which enables genome-scale
64 mapping of genetic modifications to traits of interest (15, 16). In addition, pooled library recombineering
65 approaches such as CRISPR-enabled trackable genome engineering (CREATE) have combined
66 CRISPR-Cas9 gene editing schemes with barcode tracking to enable high-throughput mutational
67 profiling at single-nucleotide resolution on a genome-wide scale. (17).

68

69 Meanwhile, techniques such as multiplex automated genome engineering (MAGE) have been
70 developed to generate complex mutagenesis libraries by extending recombineering to simultaneously
71 modify multiple genetic loci through iterative cycles of single-strand DNA (ssDNA) oligonucleotide
72 recombination (18). MAGE has enabled several genome-scale recombineering efforts such as the
73 recoding of all 321 occurrences of TAG stop codons with synonymous TAA codons in a single *E. coli*
74 strain (19, 20), the removal of all instances of 13 rare codons from 42 highly expressed essential genes
75 to study genome design constraints (21), the insertion of multiple T7 promoters across 12 genomic
76 operons to optimize metabolite production (22), and the His-tagging of 38 essential genes that encode
77 the entire translation machinery over 110 MAGE cycles for subsequent *in vitro* enzyme studies (23). In
78 addition, methods such as tracking combinatorial engineered libraries (TRACE) have been developed
79 to facilitate the rapid, high-throughput mapping of multiplex engineered modifications from such
80 genomic explorations to phenotypes of interest (24, 25).

81
82 To achieve the high levels of recombination necessary to carry out large-scale, multiplexed genome
83 editing, many of these studies required the use of mutagenic strains. Specifically, the endogenous
84 methyl-directed mismatch repair (MMR) system, which acts to revert newly made recombineering
85 modifications when active, was removed to more effectively retain targeted modifications in the standard
86 MAGE strain EcNR2. While deactivation of the MMR dramatically enhances recombination efficiency,
87 it also increases the rate of background mutagenesis by 100-1000 fold (26, 27). Indeed, in converting
88 all 321 occurrences of TAG stop codons to TAA stop codons, Lajoie *et al.* noted the addition of 355
89 unintended (i.e. off-target) mutations after the final strain construction (20).
90
91 Several approaches have been proposed to circumvent the use of MMR-deficient strains and thus avoid
92 their high basal rates of off-target mutagenesis. Designs utilizing mismatches that are poorly repaired
93 or that introduce silent mismatches near the desired mutation can be used to evade MMR, which only
94 recognizes short mismatches (28). Furthermore, oligos containing chemically modified bases can be
95 used to evade MMR correction and increase allelic-replacement efficiency (29). While these
96 approaches boost recombination rates without increasing basal mutagenesis rates, they either limit the
97 range of mutations that can be implemented or significantly increase oligonucleotide costs.
98
99 More recent efforts have focused on approaches to create a transient mutagenesis state. Specifically,
100 cells are cycled between phases of elevated mutation rate, during which editing can take place
101 efficiently, and phases of wild type-like mutation rates, during which cells can be propagated without
102 incurring a significant number of background mutations. Nyerges *et al.* reported the use of a
103 temperature-controlled mismatch repair deficient strain (*E. coli* tMMR) in which the MMR machinery can
104 be transiently inactivated by shifting cells to a non-permissive temperature (36°C) during oligonucleotide
105 incorporation and cell recovery and then reactivated by returning cells to the permissive temperature
106 (32°C) for propagation (30). While this approach reduces the number of off-target mutations by 85%, it
107 restricts cell growth to 32°C and hence increases the time between recombineering cycles. In contrast,
108 Lennen *et al.* developed a plasmid-based MAGE system, Transient Mutator Multiplex Automated
109 Genome Engineering (TM-MAGE). In TM-MAGE, *E. coli* Dam methylase is inducibly overexpressed to
110 transiently limit MMR and thus enable high allelic replacement efficiencies with a 12- to 33-fold lower
111 off-target mutation rate than strains with fully disabled MMR (31).
112
113 Given existing approaches to recombineering in *E. coli*, researchers still face a trade-off between high-
114 efficiency genome editing and genome stability. Here we present a rational genome engineering
115 approach to develop such a platform strain, called BioDesignER, with enhanced recombineering
116 efficiency while retaining low off-target mutagenesis rates and enabling short editing cycle times. We
117 refactored the λ-Red machinery in *E. coli* K-12 MG1655-derived EcNR1 to decrease cycle time and
118 reduce toxicity, stacked genetic modifications shown to increase recombination rates, and
119 characterized gene expression across the chromosome at curated integration loci, herein referred to as
120 Safe Sites. We also introduced genomic modifications to independently control four transcriptional

121 regulators of gene expression and characterized the induction regime for each regulator. We profiled
122 the growth and ssDNA recombination rates of BioDesignER with a dual-fluorescent reporter cassette
123 integrated at each Safe Site and also demonstrated the retention of double-strand DNA (dsDNA)
124 recombination capabilities in the strain. We performed a comparative study of background mutagenesis
125 rates of our strain and alternative platform strains using a fluorescent reporter-based fluctuation assay
126 and found that BioDesignER exhibited a 4.2-fold lower mutagenesis rate compared to the widely used
127 recombineering strain EcNR2. Finally, we compared the multi-cycle accumulation of targeted mutations
128 for BioDesignER and other high-efficiency recombineering strains and found that BioDesignER
129 exhibited similar multiplex editing efficiencies to EcNR2.nuc5-, a persistent mutator strain with the
130 highest reported ssDNA recombination efficiency. BioDesignER is a high-fidelity genome engineering
131 strain that uniquely enables high-efficiency recombineering while retaining low basal mutagenesis rates.
132

133 MATERIALS AND METHODS

134 Chemicals, reagents, and media

135 LB Lennox Medium (10 g/L Tryptone, 5 g/L Yeast Extract, 5 g/L NaCl; Sigma Aldrich, USA) was used
136 to culture strains for experiments, to prepare electrocompetent cells for recombineering, and as
137 recovery broth following electroporation. Antibiotics concentrations used were 34 μ g/mL for
138 chloramphenicol, 100 μ g/mL for carbenicillin, and 50 μ g/mL for kanamycin. Anhydrotetracycline (CAS
139 13803-65-1; Sigma Aldrich, USA) was used at 100 ng/mL to induce the λ -Red genes for
140 recombineering. For *thyA*-mediated recombineering steps, M9 minimal media supplemented with 0.4%
141 glucose, 0.2% casamino acids, thymine (100 μ g/mL), and trimethoprim (50 μ g/mL) was used. M9
142 minimal media with valine (20 μ g/mL) was used to select for the *i/vG⁺* genotype. All M9 minimal media
143 was supplemented with biotin at 10 μ g/mL to account for the biotin auxotrophy common to all EcNR1-
144 derivative strains.

145 Oligonucleotides

146 Oligos were ordered from Integrated DNA Technologies (IDT), resuspended in 1x TE buffer at either
147 500 μ M (recombineering oligos) or 100 μ M (standard amplification oligos), and stored at -20°C. For
148 recombineering workflows, oligos were designed to target the lagging strand of DNA replication and
149 contain at least 35 bp of homology to the target locus. Oligos for testing recombination efficiency were
150 ordered with 5' phosphorothioate base modifications. Oligo sequences for individual lineage
151 construction steps are available in linked Benchling files from Supplementary Table S1.

152 Strains

153 Relevant strains used in this work are reported in Table 1. Supplementary Table S2 provides relevant
154 genotypes of 32 intermediate strains in the lineage between EcNR1 to BioDesignER. This table includes
155 descriptions of genetic modifications, associated recombineering, selection and enrichment methods,
156 and a web link to sequence-level detail of each modification. Supplementary Table S3 provides a
157 summary of strain identification numbers and genotypes for the BioDesignER lineage.

158 Growth rate measurements

159 Two clones of each strain were cultured overnight in LB Lennox (LB) medium with chloramphenicol.
160 The following morning each strain culture was back-diluted 1:100 into two media types: (1) LB with aTc
161 (LB+aTc) (2) LB. The resulting inocula were divided into four technical replicates and then grown for up
162 to 18 hours in a Biotek Synergy 2 microplate reader. The growth rate at early exponential phase was
163 calculated from the resulting optical density data using custom analysis scripts in python.

164 Competent cell preparation and recombineering

165 Strains were grown overnight in LB Lennox medium (LB) with antibiotics as appropriate at 37°C. The
166 following morning each strain culture was back-diluted 1:100 into 25 mL LB+aTc and grown at 37°C
167 until they reached OD600 0.3-0.4. The resulting mid-log cultures were chilled in a 4°C ice-water bath.
168 Cultures were centrifuged (Beckman-Coulter Allegra 25R) at 8000 xg and subjected to two washes: (1)
169 25 mL chilled water (2) 15 mL chilled 10% glycerol. The cell pellets after the final glycerol wash were
170 resuspended in 10% glycerol, yielding approximately 500 uL of competent cells given the residual cell
171 mass from the wash.

172 Due to their different induction and growth requirements, EcNR2 and EcNR2.nuc5- strains were grown
173 overnight at 30°C, back-diluted 1:100 into 25 mL LB+chlor media, and cultured at 30°C until they
174 reached OD600 0.3-0.6. The λ-Red machinery was induced by incubating the cultures in a 42°C water
175 bath for 15 minutes after which the strains were chilled in a 4°C ice-water bath for at least 10 minutes.
176 The remainder of the preparation for EcNR2 and EcNR2.nuc5- follows the same aforementioned wash
177 steps.

178 40 uL of competent cells were used for each recombineering reaction. Oligos were diluted to 50 uM
179 concentration in 10% glycerol and 10 uL of the diluted oligo was added to the competent cell mixture.
180 For water control reactions, 10 uL of water was added. For multiplexed reactions, 10 uL of a cocktail
181 with a total oligo concentration of 50 uM was used. The resulting cell-oligo mix was transferred to a
182 chilled cuvette (1 mm gap, VWR) and electroporated using a BTX™-Harvard Apparatus ECM™ 630
183 Exponential Decay Wave Electroporator with the following parameters: voltage (1800 V), resistor (250
184 Ω), capacitor (25 uF).

185 **Fluorescence-coupled scar-free selection/counter-selection**

186 Working from the *ΔthyA* strain RE095 and derivative strains (Supplementary Table S2), a dsDNA *thyA*
187 cassette with or without a fluorescence gene (Supplementary Figure S1) was amplified with 35-50 bp
188 homology to a target genomic locus and integrated via standard recombineering as described above,
189 with the exception that cells were made competent by growing in LB supplemented with thymine (100
190 µg/mL) and trimethoprim (50 µg/mL). Integrants of *thyA* were selected for on LB media. Colonies with
191 fluorescence-coupled *thyA* cassettes were screened visually for fluorescent phenotypes on a blue-light
192 transilluminator. Proper insertion of the cassette was confirmed by locus-specific colony PCR.
193 Replacement of the *thyA* cassette was performed through recombineering with a ssDNA or dsDNA
194 cassette as described in Supplementary Table S2 and selected for on M9 agar plates supplemented
195 with thymine (100 µg/mL), trimethoprim (50 µg/mL), and casamino acids (0.2%). Removal of
196 fluorescence-coupled *thyA* cassettes was screened visually for non-fluorescent colonies via blue-light
197 transillumination and sequences were validated via colony PCR and Sanger sequencing.

198 **Recombineering efficiency and Safe Site expression measurements**

199 Competent cells were transformed with water (control) or oligos to turn off sfGFP, mKate2, or both
200 reporters. Following electroporation, cells were resuspended in 3 mL LB+carb. These cultures were
201 mixed and 30 uL was transferred into an additional 3 mL LB+carb for overnight growth at 37°C (or 30°C
202 for EcNR2 and EcNR2.nuc5-). The following morning, saturated cultures of each transformation were
203 diluted 1:200 into Phosphate-buffered saline (PBS) solution and run on a Sony SH800 cell sorter for
204 single-cell flow cytometry analysis. At least 50,000 events were recorded for each reaction, and the
205 fractional abundance of each reporter phenotype (GFP+ RFP+, GFP- RFP+, etc.) in the population was
206 measured. The threshold for each reporter phenotype was determined via a prior calibration in which
207 gates for each fluorescent reporter were measured. For measurement of gene expression across Safe
208 Sites, overnight outgrowths of control reactions from the Safe Site recombineering efficiency
209 transformations were processed on the flow cytometer.

210 **Response curves of inducible regulators**

211 BioDesignER was transformed with plasmids containing a GFP gene regulated by each transcription
212 factor - AraC (pBAD), CymR (pCym), or LacI (pLac) - and controlled by one of two replication origins,
213 p15A or pSC101. Plasmids with the p15A origin contain a *kanR* marker and plasmids with the pSC101
214 origin use a *cmR* marker. Plasmid sequences are available via Benchling
215 (<https://benchling.com/organizations/arkinlab>). Individual colonies were inoculated in LB with an
216 appropriate antibiotic to maintain the plasmid and grown overnight. Saturated cultures were diluted 200-
217 fold into a microtiter plate (Corning 3904) and grown at 37°C with shaking in a Biotek H1 plate reader.

218 Kinetic growth and fluorescence measurements were taken every 5 or 10 minutes for 12 hours.
219 Absorbance was measured at 600 nm. GFP fluorescence was measured using 485/20 nm and 520/15
220 nm filter cubes for excitation and emission, respectively. mKate fluorescence was measured using
221 560/20 nm and 615/30 nm filter cubes for excitation and emission, respectively. Fluorescence values
222 measured nearest OD 0.5 were used to estimate absorbance-normalized fluorescence in each channel.

223 **Flow cytometry analysis of inducible regulators**

224 Saturated cultures from the kinetic growth assays used to measure regulator inducer responses were
225 diluted 400-fold into PBS and analyzed in a BD LSR Fortessa flow cytometer (488 nm excitation / 525/50
226 nm emission for GFP; 561 nm excitation / 670/30 nm emission for mKate) using an autosampler. Raw
227 .fcs files were imported for pre-processing and subsequent analysis with custom Python scripts (see
228 Supplementary Data D1 for example) using the FlowCytometryTools software package
229 (<https://github.com/eyurtsev/FlowCytometryTools>). For each sample, 50,000 events were captured and
230 outliers in forward scatter and side scatter were removed using a filter with cut-offs for events outside
231 the second and third quartile.

232 **Safe Site expression analysis**

233 Data for expression levels at each Safe Site were calculated from flow cytometry data and used to
234 measure recombineering efficiency at each Safe Site. Data files were extracted for four recombineering
235 conditions (no oligo control, GFP-off, mKate-off, and dual-off) and two biological replicates. The
236 geometric mean for each fluorescence channel was calculated from filtered data. Specifically, events
237 outside the second and third quartiles for forward and side scatter channels were removed from analysis
238 for each .fcs data file. The dual-fluorescent subpopulation for each measurement was extracted by
239 gating at a value that excluded recombinant, non-fluorescent subpopulations but did not truncate the
240 distribution of the dual-fluorescent subpopulation.

241 **Fluctuation assay**

242 Fluctuation tests were performed on an inactivated *cmR-mNeon* translational fusion cassette integrated
243 at Safe Site 1. The cassette was inserted using selection on chloramphenicol and subsequently
244 inactivated for the following strains: pTet-λ, damOE, dnaG.Q + ΔrecJ/ΔxonA, BioDesignER, pTet-λ
245 ΔmutS, and EcNR2. The inactivated cassette was first integrated as double-strand DNA into the
246 respective strains via recombineering and selected for by plating on LB agar supplemented with 34
247 µg/mL chloramphenicol. A premature stop codon (AAA to TAA) was inserted into *cmR-mNeon* via
248 single-strand DNA recombineering with an oligo harboring the stop codon mutation. The non-
249 fluorescent population was enriched using cell sorting (Sony SH800) and the sorted cells were plated
250 on LB agar plates.

251 Prior to fluctuation tests, individual non-fluorescent colonies were grown at 30°C in LB+carb and stored
252 at -80°C as glycerol stocks normalized to OD600 of 0.5. For the fluctuation tests, cultures were diluted
253 1000-fold and grown for 16 hours in permissive conditions of LB+carb at 30°C (N=24). For pTet-λ
254 ΔmutS, EcNR2, and EcNR2.nuc5-, 20µL of culture was spotted onto LB agar plates supplemented with
255 chloramphenicol and carbenicillin. For all other strains, 100 µL volume spots were used. Viability counts
256 were estimated for all strains by serial dilutions of 6 independent cultures on LB agar plates
257 supplemented with carbenicillin. Chloramphenicol-resistant mutants were counted and mutation rates
258 were inferred by the MSS-MLE method (32, 33).

259 **Iterative recombineering cycling**

260 Strains were prepared for transformation using the competent cell protocol described above using 25
261 mL of culture with a target OD600 of 0.3. Each culture was resuspended in ~500 µL of 10% glycerol
262 after washes. Each transformation consisted of 40 µL competent cells mixed with 10 µL of 50 µM oligo
263 mix. After transformation, cells were recovered in 3 mL LB supplemented with carbenicillin. The
264 recovery culture was grown to saturation before beginning the next round of competent cell prep and
265 recombination. In parallel, the recovery culture was diluted 1:60 into an additional 3 mL of LB
266 supplemented with carbenicillin and grown to saturation prior to measurements using flow cytometry
267 (Sony SH800).

268

269 **RESULTS**

270 **Rational strain design**

271 We introduced multiple targeted modifications to an MG1655-derivative strain to decrease
272 recombination cycle time, reduce toxicity of the recombination machinery, and introduce a transient
273 hypermutation phenotype via hypermethylation (Figure 1A-B, Table 1). Using EcNR1 (18) as the host,
274 we refactored the λ -Red recombination machinery, which consists of the genes *exo*, *bet*, and *gam*, and
275 serves as the basis for mediating homology-directed recombination of ssDNA and dsDNA products. To
276 reduce recombineering cycle times, we replaced the temperature-inducible regulation of the λ -Red
277 locus with a TetR-regulated design (Figure 1C). This allowed us to propagate cells at 37°C instead of
278 30-32°C during all phases of a recombineering workflow: competent cell prep, λ induction, cell recovery,
279 and selection. We also minimized the λ prophage by deleting the λ -*kil* gene, which has been reported
280 to be responsible for the cell death phenotype observed under λ -Red expression (34), and other
281 dispensable phage genes. Finally, we introduced DNA adenine methyltransferase (*dam*) to the λ -Red
282 operon of our strain. Co-induction of *dam* with the λ -Red recombination genes results in transient
283 hypermutation via hypermethylation, which has been reported to enable incorporated mutations to
284 evade MMR (31).

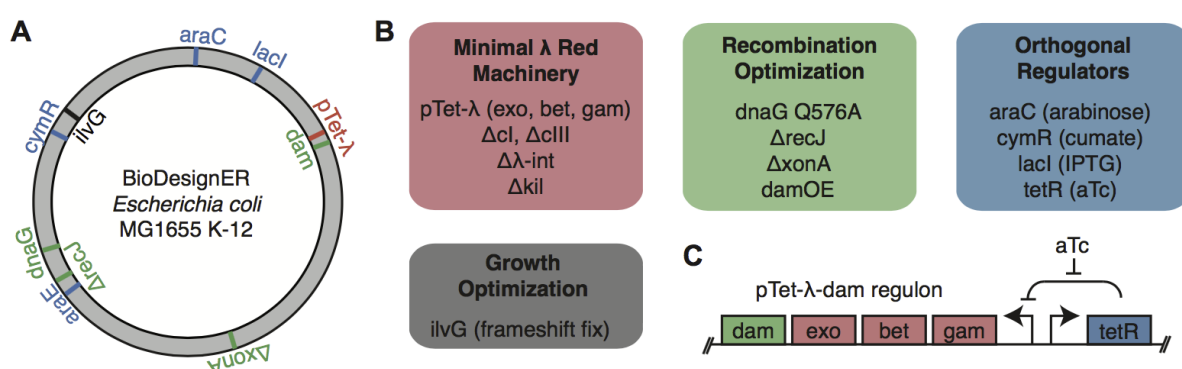


Figure 1. Overview of modifications in BioDesignER. (A) Chromosome map of the BioDesignER strain (derived from *E. coli* MG1655 K-12) with modifications made in the platform strain mapped to corresponding positions on the genome. (B) Functional grouping of genomic modifications based on purpose in platform strain (e.g. minimization of λ -Red machinery, optimization of recombination efficiency, implementation of multiple orthogonal regulators, or optimization of growth). (C) Genetic architecture of refactored λ -Red machinery and *dam* overexpression construct along with regulation by TetR.

285

286 To remove a valine-sensitive growth defect present in *E. coli* K-12, we restored expression of *ilvG*. K-
287 12 contains three acetohydroxy acid synthases (*ilvB*, *ilvG*, *ilvH*) that are involved in branch-chained
288 amino acid biosynthesis. K-12 does not express *ilvG* due to a natural frameshift mutation and thus
289 exhibits a growth defect in the presence of exogenous valine and the absence of isoleucine (35, 36).
290 This valine-sensitive growth phenotype is alleviated by restoration of *ilvG* (37). Using oligo-mediated
291 recombination (Methods) we removed the frameshift mutation in the endogenous *ilvG* gene, which has
292 been reported to enable faster growth in minimal media. We called this strain pTet-λ.

293 We next incorporated genomic modifications shown to improve recombination efficiency. Using a scar-
294 free genome engineering workflow that utilizes a novel *thyA* selection/counter-selection cassette
295 containing a fluorescent marker (Supplementary Figure S1, Methods), we iteratively generated multiple

296 beneficial mutations. For example, genetic variants of DNA primase (*dnaG*) enhance recombination
297 efficiency by increasing the length of Okazaki fragments, thus exposing longer stretches of the lagging
298 strand of the replication fork to ssDNA recombination (38). We incorporated the *dnaG*.Q576A variant,
299 which was shown to boost recombination efficiency more than other *dnaG* mutants in EcNR2, into our
300 strain.

301 Endogenous nucleases can degrade exogenous DNA used in recombineering workflows. The removal
302 of a set of five nuclease genes (*endA*, *exoX*, *recJ*, *xonA*, *xseA*) has been shown to improve ssDNA
303 recombination efficiency (39). However, while this exonuclease knockout strain, EcNR2.nuc5-,
304 exhibited increased recombination efficiency, it also resulted in a lower post-electroporation growth rate
305 compared to EcNR2. This suggested that deletion of the entire set of nucleases introduces to the strain
306 an undesirable physiological defect. To avoid such growth defects, which are compounded for
307 workflows requiring multiple recombineering cycles, we looked to systematically combine exonuclease
308 knockouts that distinctly improve recombination rates. We constructed individual knockouts of each of
309 the five exonucleases and measured the recombineering efficiency of the resulting strains. We assayed
310 recombination efficiency for each exonuclease knockout using oligo mediated recombination at a
311 genetically-encoded *sfGFP* reporter. In this assay, recombination of an oligo designed to introduce a
312 premature stop codon into *sfGFP* results in a loss of fluorescence that can be quantified using flow
313 cytometry. Deletions of *xonA* (4.2%) and *recJ* (2.6%) showed the greatest efficiencies, while the
314 remaining exonuclease deletions yielded nominal efficiencies (<1%) (Supplementary Table S4). Based
315 on these results, we deleted only two of the five exonucleases (*recJ*, *xonA*) in the next step of strain
316 construction. While deletion of the λ-Red exonuclease (*exo*) can also promote stability of exogenous
317 ssDNA (39), we opted to retain it due to its role in dsDNA recombination. The culmination of these
318 genetic modifications in addition to the inducible regulator modifications described below, resulted in
319 the BioDesignER strain.

320 To assess the effect of BioDesignER modifications on strain fitness, we measured the growth rates of
321 key strains in the modification lineage in LB rich media (Figure 2A). We noted that, in general, doubling
322 times decreased as additional modifications were made. Additionally, in contrast to cell death reported
323 for extended co-expression of λ-*kil* with the recombination machinery (34), we observed only a slight
324 increase in doubling time when expressing the refactored λ-Red cassette.

325 **BioDesignER recombineering enhancements**

326 ssDNA recombination enhancements: To quantify recombineering enhancements of key BioDesignER
327 modifications, we measured ssDNA recombination rates for several strain intermediates. We integrated
328 a dual fluorescent reporter cassette expressing both *sfGFP* and *mKate2* at a common genomic locus
329 for each strain of the lineage and quantified ssDNA recombination efficiency. For each strain we
330 transformed an oligo to inactivate *sfGFP* via incorporation of a premature stop codon. We also
331 performed a control reaction in each case using water in place of oligo. After recovery and outgrowth
332 we measured the fluorescence profiles of each strain using flow cytometry (Figure 2B). We observed

333 increases in recombination efficiency at each modification stage with single cycle conversion rates
334 improving from 1.6±0.1% (mean ± 1 standard deviation) in pTet-λ to 25.4±1.0% in BioDesignER.

335 To investigate the efficacy of mismatch repair evasion on recombination efficiency, we compared
336 BioDesignER against pTet-λ derivative strains containing mismatch repair modifications and against
337 two standard $\Delta mutS$ recombineering variants, EcNR2 and EcNR2.nuc5-. BioDesignER (25.4±1.0%)
338 exhibits much higher recombination efficiency than pTet-λ with *dam* over-expression (damOE,
339 6.91±0.19%) or $\Delta mutS$ (12.9±1.7%) as hypermutagenesis strategies (Figure 2C, left panel). Performing
340 the same recombineering experiments at 30°C and comparing to EcNR2 and EcNR2.nuc5-, which are
341 constrained to growth at 30°C, we found that BioDesignER (13.6±1.2%) exhibited recombination rates
342 comparable to EcNR2 (14.5±2.1%), yet approximately three-fold lower than EcNR2.nuc5- (37.7±3.8%)
343 (Figure 2C, right panel). We were surprised to find that the recombineering efficiency of BioDesignER
344 decreased by nearly two-fold when grown at a lower temperature.

345 **dsDNA recombination enhancements:** Knocking out endogenous exonucleases has been reported to
346 significantly reduce or abolish dsDNA recombination efficiency (39). We measured the efficiency of
347 dsDNA recombination in pTet-λ and BioDesignER and found no significant reduction in recombination
348 efficiency (Figure 2D). This suggests that λ-exo is sufficient to process dsDNA recombination templates
349 in the absence of multiple host exonucleases. A previous study reported that dsDNA recombination is
350 at least an order of magnitude less efficient in a four-nuclease deficient genotype ($\Delta exoX, \Delta recJ, \Delta xseA,$
351 $\Delta xonA$) with abolished dsDNA recombination activity in a three-nuclease ($\Delta recJ, \Delta xseA, \Delta xonA$)
352 knockout (39). We note here that we were successful in generating dsDNA recombinants in
353 EcNR2.nuc5- at a similar efficiency to EcNR2 with no alteration to the recombineering protocol,
354 suggesting that another nuclease is aiding dsDNA recombination in *E. coli* or that recombination can
355 occur through an exonuclease-independent mechanism.

356 **Table 1.** Genotypes of abbreviated strains.

Strain	Relevant genotype	Reference
EcNR1	MG1655 λ-Red(<i>ampR</i>):: <i>bioA/bioB</i>	Wang <i>et al.</i> 2009
EcNR2	EcNR1 <i>cmR</i> :: <i>mutS</i>	Wang <i>et al.</i> 2009
EcNR2.nuc5-	EcNR2 <i>dnaG.Q576A ΔrecJ ΔxonA ΔxseA ΔexoX Δreda</i>	Mosberg <i>et al.</i> 2012
pTet-λ	MG1655 pTet2- <i>gam-bet-exo-tetR/ampR::bioA/B ilvG⁺</i>	This study
damOE	MG1655 pTet2- <i>gam-bet-exo-dam-tetR/ampR::bioA/B ilvG⁺</i>	This study
exo1	pTet-λ <i>dnaG.Q576A</i>	This study
exo2	pTet-λ <i>ΔrecJ ΔxonA</i>	This study
BioDesignER	damOE <i>dnaG.Q576A ΔrecJ ΔxonA Pcp8-araE ΔaraBAD pConst-araC lacIQ1 cymR::SafeSite7</i>	This study

358 **Control of multiple independent regulators**

359 BiodesignER expresses transcriptional regulators that utilize four independent small-molecule inducers
360 to allow multi-input control of synthetic circuits, biosynthetic pathways, or gene editing tools. The strain
361 produces the repressors TetR, LacI and CymR as well as the activator AraC. TetR is expressed from
362 the λ prophage element native to EcNR1. We incorporated the transcriptional overexpression allele
363 *lacI^{Q1}* to boost LacI production, which allows efficient regulation of multi-copy plasmids (40). We also
364 introduced the tight and titratable regulator CymR (41), which is inactivated by the small molecule
365 cumarate. To improve gene regulation by arabinose we replaced the arabinose-sensitive promoter of the
366 *araE* transporter gene with a constitutive promoter to eliminate all-or-none expression and allow
367 titratable induction (42). In conjunction with this modification, we introduced a constitutive promoter to
368 drive expression of AraC and deleted the *araBAD* operon to eliminate arabinose degradation via
369 catabolism.

370 To characterize the induction profiles of each regulator, we quantified the fluorescence levels and
371 growth rates of cells transformed with multi-copy plasmids. We constructed a set of GFP expression
372 plasmids with promoters responsive to each regulator (Figure 2E, see Supplementary Figure S2 for
373 sequence-level details) and transformed each plasmid into BioDesignER. Gene expression profiles
374 were characterized by measuring single-cell fluorescence and bulk growth and fluorescence.

375 Fold-change induction for each regulator increased with plasmid copy number while no leaky
376 expression was observed for low-copy and medium-copy plasmids. For plasmids with low-copy
377 replication origin pSC101, we observed mean fold-change induction levels of 107, 68, and 20 for
378 arabinose, cumarate, and IPTG, respectively. For plasmids with medium-copy replication origin p15A, we
379 observed mean fold change induction levels of 146, 184, and 30 for arabinose, cumarate, and IPTG,
380 respectively. In both copy-number contexts, GFP expression with no inducer was indistinguishable from
381 a control plasmid lacking *gfp*. We found that repressor levels were insufficient to fully repress GFP
382 expression on plasmids with the ColE1 replication origin. We note that AraC-regulated GFP expression
383 saturates near 33 μ M (5 μ g/mL, 0.0005%) arabinose, a much lower saturation point than common
384 plasmid-based systems (0.1% arabinose).

385 Single-cell distributions observed through flow cytometry revealed unimodal distributions of GFP
386 expression for nearly all induction conditions (Figure 2E). GFP expression from both cumarate- and IPTG-
387 responsive promoters produced monotonic, decreasing coefficient of variation noise profiles for
388 increasing inducer levels (Supplementary Figure S3). For arabinose induction, despite introducing
389 modifications consistent with Khlebnikov *et al.*, we observed significant cell-cell variability at two
390 intermediate arabinose levels. Specifically, we observed a maximum coefficient of variation at 3.3 μ M
391 (Supplementary Figure S3), manifest in Figure 2E as the broad, weakly bimodal fluorescence
392 distribution.

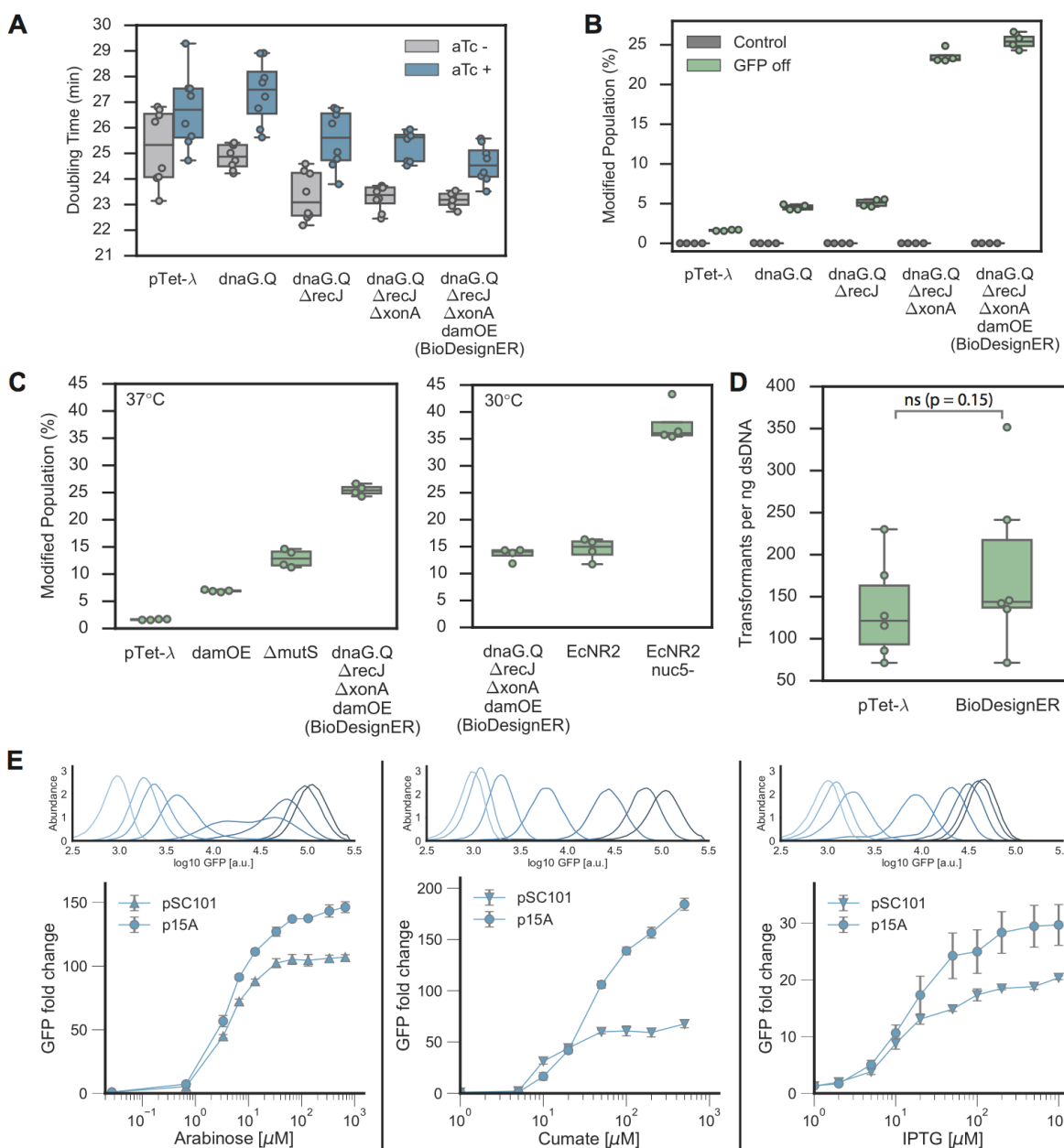


Figure 2. Strain Characterization **(A)** Doubling times of strains grown at 37°C for selected strains of BioDesignER lineage starting with the strain harboring pTet-λ. Additional modifications shown moving to the right. Doubling times reported for strains grown with (blue) and without (gray) aTc induction to show the effect of λ-Red expression on growth. Data represented as boxplots overlaid with corresponding data points. **(B)** ssDNA recombination enhancements for the strain lineage as measured via flow cytometry to measure the population fraction in which an sfGFP reporter could be turned off via incorporation of a premature stop codon. **(C)** The recombination efficiency of BioDesignER compared to pTet-λ harboring modifications that interfere with mismatch repair (damOE, ΔmutS) (left, 37°C) and to canonical recombining strains such as EcNR2 and EcNR2.nuc5- (right, 30°C). **(D)** Transformation efficiency of BioDesignER compared to pTet-λ (control) to show retention of dsDNA recombination efficiency. P-value from Mann-Whitney U-test; ns - not significant. **(E)** Flow cytometry traces (top) with corresponding fold-change response curves (bottom) for each inducible, orthogonal regulator. Inducer concentrations used for flow cytometry traces are: 0, 0.33, 0.67, 1.3, 3.3, 6.7, 33, 130 μM (arabinose); 0, 2, 5, 10, 20, 50, 100 μM (cumate); 0, 1, 2, 5, 10, 20, 50, 500 μM (IPTG).

393

394 **Characterization of genomic integration Safe Sites**

395 Genome Integration Safe Sites: To aid identifying genomic loci that provide reliable gene expression
 396 and recombination efficiency for future engineering efforts, we characterized a curated list of integration
 397 loci across the *E. coli* K-12 genome. The resulting eight genomic loci, termed Safe Sites, were chosen
 398 based on several criteria to minimize disruption to local chromosomal context upon integration of
 399 synthetic DNA constructs (Figure 3A, Supplementary Figure S4). Specifically, the integration Safe Sites

400 are intergenic regions located between two convergently transcribed, non-essential genes that do not
401 exhibit any phenotypes or growth defects across the majority of biochemical conditions screened in
402 previous high-throughput studies (14, 43) (Supplementary Table S5), and contain no annotated features
403 (small RNAs, promoters, transcription factor binding sites) according to RegulonDB (44)
404 (Supplementary Table S6).

405 To characterize gene expression variation across the chromosome, we measured the expression of
406 dual-fluorescent reporters (*sfGFP*, *mKate2*) integrated into BioDesignER at each Safe Site. We
407 observed a linear decrease in expression for both *sfGFP* (pearson $r_{sfGFP,arm1} = -0.91$, pearson $r_{sfGFP,arm2} = -0.65$, $p_{sfGFP} < 0.05$, permutation test) and *mKate2* (pearson $r_{mKate,arm1} = -0.85$, pearson $r_{mKate,arm2} = -0.51$, $p_{mKate} < 0.05$, permutation test) reporters with respect to distance from the chromosomal origin
409 (Figure 3B). This result was consistent with expected variations in local chromosomal copy number due
410 to bi-directional replication dynamics during growth (45, 46). Interestingly, we observed a much stronger
411 correlation of expression to distance from replication origin for chromosome Arm 1, though *mKate2*
412 expression at Safe Site 8 was a low outlier. We also assessed the effect of integration at each Safe Site
413 on cellular fitness by measuring growth rates for each integration strain. We observed that, in general,
414 genomic integration and expression from each Safe Site did not reduce growth rate, though Safe Site
415 8 displayed a nominal decrease when grown under aTc induction (Supplementary Figure S5). The two
417 unexpected results at Safe Site 8 suggest that it may not be a reliable locus for integration.

418 Recombination Rates across Safe Sites: Changes in local chromosomal structure may lead to
419 unexpected fluctuations in recombination efficiency at various locations across the genome. To
420 characterize recombination efficiency as a function of chromosomal locus for BioDesignER, we
421 performed three independent ssDNA oligo-mediated recombination reactions for the panel of eight Safe
422 Site strains. For each strain we independently transformed (1) an oligo to inactivate *sfGFP*, (2) an oligo
423 to inactivate *mKate2*, or (3) an oligo cocktail to inactivate both reporters. We also performed a control
424 reaction in each case using water in place of oligo. For Safe Sites that lie on opposite sides of the
425 replication fork, we designed appropriate oligos to ensure recombination targeting the lagging strand.
426 We found that recombination rates were consistently high across the chromosome with Safe Sites
427 displaying single cycle, single site conversion rates of $17.0 \pm 6.70\%$ and $19.7 \pm 5.7\%$ for *sfGFP* and
428 *mKate2*, respectively (Figure 3C). We also report single cycle, multiplex conversion rates of $7.5 \pm 4.4\%$
429 for the *sfGFP*, $7.9 \pm 2.9\%$ for the *mKate2*, and $6.3 \pm 2.3\%$ for both reporters when transformed with the
430 dual oligo cocktail.

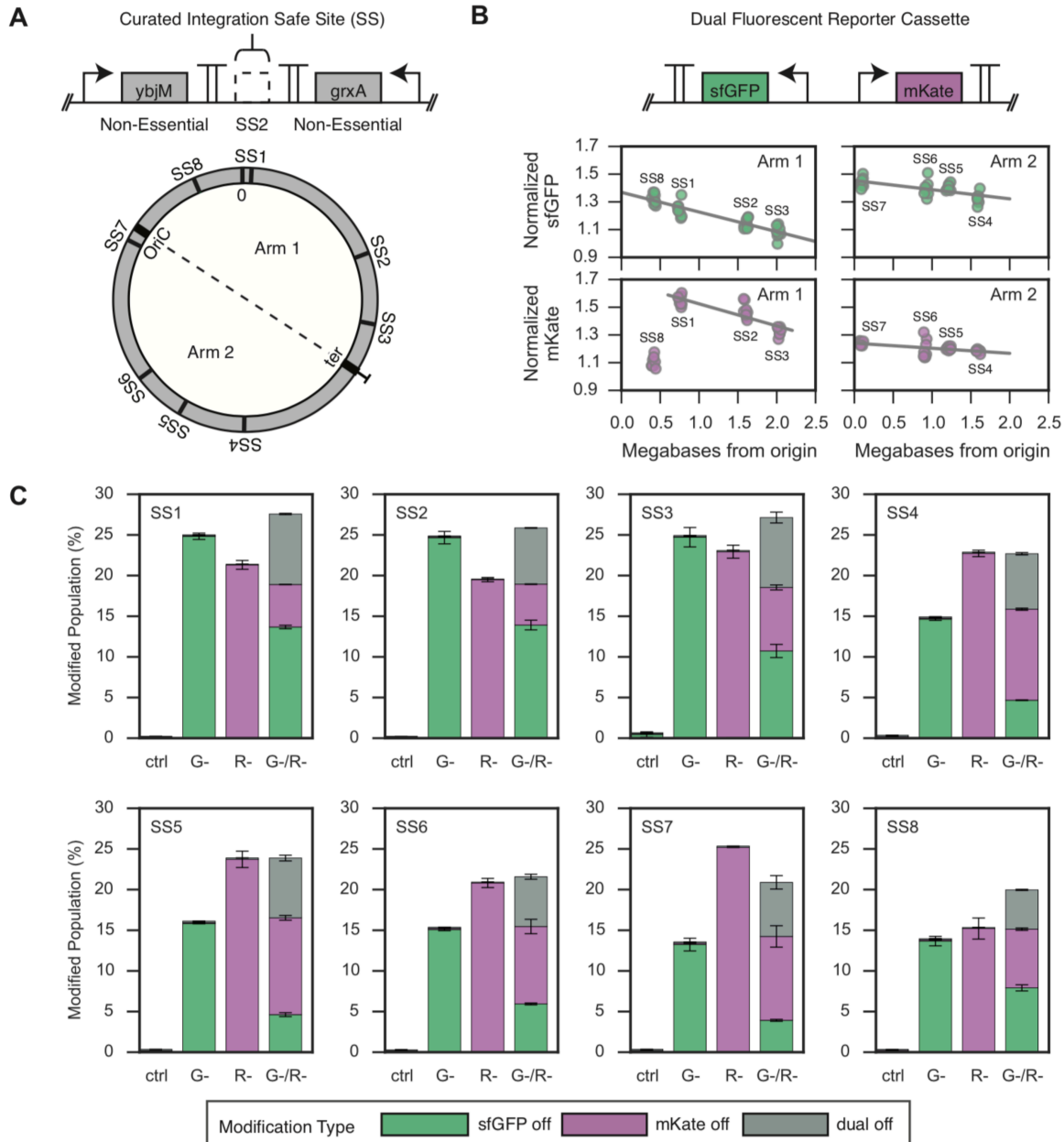


Figure 3. Recombination Characterization **(A)** Circular map of the BioDesignER chromosome with Safe Sites mapped to corresponding genome position and chromosomal arm (replicore). **(B)** Genetic architecture of dual fluorescent reporter construct (top) and observed expression of reporters when integrated at each Safe Site on the chromosome (bottom). Replicate measurements of normalized expression levels for each reporter arrayed by chromosomal arm on which construct is integrated. **(C)** ssDNA recombination rates at each Safe Site for four independent recombineering reactions. X-axis denotes transformed oligo(s) (G- for sfGFP, R- for mKate) or ctrl (water). Bar height corresponds to the mean of two measurements and error bars represent span of data. Stacked barplots for each reaction represent population fractions containing one of three possible modifications (sfGFP off, mKate off, or dual off when both reporters inactivated).

432 **Analysis of transient hypermethylation effects on mutagenesis**

433 To investigate the effect of BioDesignER
434 modifications on global mutation rate, we
435 developed a mutagenesis detection assay
436 with a single nucleotide target. The
437 mutagenesis cassette utilizes
438 chloramphenicol acetyltransferase (*cat*)
439 gene translationally fused to green
440 fluorescence gene *mNeon* (Figure 4A). This
441 strategy allows estimation of mutation rate
442 without mutant fitness biases and second-
443 site suppressor mutations observed in
444 traditional fluctuation analyses such as
445 rifampicin resistance (47). Following
446 integration of the mutagenesis cassette at
447 Safe Site 1, we introduced a TAA stop
448 codon at Lys19 of *cat* via a single nucleotide
449 mutation. Only mutations that convert the
450 stop codon to alternate codons generate
451 chloramphenicol resistant, green
452 fluorescent colonies, thus eliminating the
453 possibility of suppressor mutations
454 occurring in the fluctuation test.

455 Using this assay, we benchmarked mutation
456 rates of BioDesignER against (1) strains in
457 the BioDesignER construction lineage, (2)
458 EcNR2 (reference), and (3) MMR-deficient
459 (control) strains pTet-λ *ΔmutS* and damOE.
460 All assayed strains utilized the inactivated
461 *cat-mNeon* cassette at Safe Site 1 as shown
462 in Figure 4A. To allow EcNR2 to be
463 compatible with the *cat-mNeon* fluctuation
464 assay, we replaced the *cmR* selection
465 cassette native to EcNR2 with *kanR*. Under
466 comparable growth conditions, we
467 estimated mutation rates of 3.36×10^{-9}
468 nucleotides/genome/replication, 4.55×10^{-9} (CI: 3.10-6.19×10⁻⁹), and 6.54×10^{-9} (CI: 4.77-8.51×10⁻⁹) for
469 pTet-λ, damOE, and BioDesignER, respectively. By comparison, we observed mutation rates of

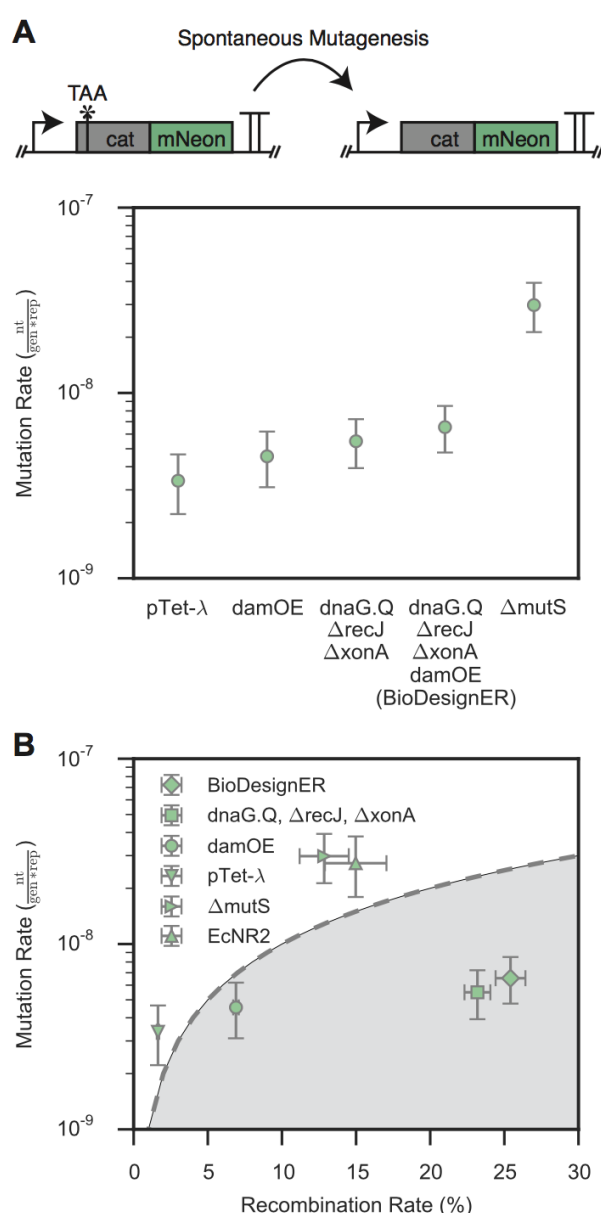


Figure 4. Mutational Analysis (A) Background mutation rates (nucleotides/genome/replication) as measured via a *cat-mNeon* fluctuation assay for various stages of BioDesignER strain construction compared to an MMR-deficient (*ΔmutS*) strain derived from pTet-λ. Error bars represent 95% confidence intervals. (B) Single-cycle ssDNA recombination efficiency plotted against background mutation rate for each strain to show tradeoffs between recombination and mutation rates. The resulting tradeoff space represents the unit increase in mutation rate observed for a unit increase in recombination rate and is divided by $y = \beta^*x$, where $\beta = 10^{-9}$ is a characteristic scaling factor for the mutation rate. X-error bars represent ± 1 standard deviation and Y-error bars represent 95% confidence intervals.

(95% confidence interval (CI): 2.22-4.66×10⁻⁹) for pTet-λ, damOE, and BioDesignER, respectively. By comparison, we observed mutation rates of

470 2.98×10^{-8} (CI: $2.13\text{-}3.93 \times 10^{-8}$) for the control pTet-λ $\Delta mutS$, which was similar to the rate of 2.73×10^{-8}
471 (CI: $1.79\text{-}3.81 \times 10^{-8}$) observed for EcNR2. For all strains assayed, all chloramphenicol-resistant colonies
472 were also fluorescent. From a set of 54 individually sequenced chloramphenicol-resistant clones, we
473 observed 8 unique genotypes arising from spontaneous mutations (Supplementary Figure S6).

474 To investigate the effect of λ-Red induction on global mutation rates and compare the mutagenic effect
475 of dam over-expression to deletion of *mutS*, we tested the mutation rates for pTet-λ, damOE, and pTet-
476 λ $\Delta mutS$ both with and without aTc induction (Supplementary Figure S6). We found no effect on global
477 mutation rates due to aTc induction (i.e. expression of the λ-Red machinery) in pTet-λ and pTet-λ
478 $\Delta mutS$. Consistent with prior work (31), we observed an increase in mutation rate for damOE under aTc
479 induction - specifically, 2.4-fold in this work. Finally, we noted that even with aTc induction damOE was
480 still less mutagenic than pTet-λ $\Delta mutS$, suggesting that BioDesignER uniquely strikes a balance
481 between on-target and off-target mutagenesis rates.

482 To quantify this balance, we compared the recombination and mutagenesis rates for a selection of
483 control strains and BioDesignER (Figure 4B). The resulting trade-off space can be divided into two
484 regimes where strains falling in the shaded region exhibit a favorable trade-off between recombination
485 rate and mutation rate. BioDesignER falls in the favorable subspace, while MMR-deficient strains such
486 as EcNR2 and the pTet-λ $\Delta mutS$ fall in the unfavorable regime above the tradeoff line. To summarize
487 this result we introduce the metric recombineering fidelity, which we define as the product of fold-
488 increase in recombination rate and fold-decrease in mutagenesis rate, each relative to EcNR2. Using
489 this metric we calculate that BioDesignER exhibits 7.3-fold greater recombineering fidelity than EcNR2
490 (1.75-fold improvement in recombination rate and 4.17-fold decrease in mutagenesis rate) (Table 2).

491 **Table 2.** Comparison of recombineering fidelity factors for relevant strains.

Strain	Recombination Efficiency	Background Mutation Rate	Recombineering Fidelity
pTet-λ	$1.6 \pm 0.1\%$	3.36×10^{-9}	0.9
EcNR2	$14.5 \pm 2.1\%$	2.73×10^{-8}	1.0
BioDesignER	$25.4 \pm 1.0\%$	6.54×10^{-9}	7.3

492 **Note:** EcNR2 data collected at 30°C, pTet-λ and BioDesignER at 37°C

493 **Multi-cycle recombineering rate enhancements**

494 High single-cycle editing efficiency enables the rapid generation of genetically diverse populations
495 using multiplexed, cyclical recombineering workflows. To assess how well BioDesignER could generate
496 a population with multiplex edits, we transformed a starting population with an oligo cocktail targeting
497 multiple sites and tracked phenotypic diversity as a function of recombineering cycle for multiple strains.

498 Specifically, we transformed BioDesignER harboring the *sfGFP-mKate2* fluorescence cassette with
499 oligos to inactivate both reporters over four sequential recombineering cycles. In parallel, we compared
500 BioDesigner to pTet-λ (Figure 5A), EcNR2, and EcNR2.nuc5- (Supplementary Figure S7) transformed
501 with the same cocktail. BioDesignER exhibited high multiplex editing efficiency with nearly 60 percent
502 of the population incorporating both edits ($58.8 \pm 3.5\%$) by the fourth recombineering cycle (Figure 5A),
503 thus outperforming EcNR2 ($15.9 \pm 3.0\%$) and showing similar efficiency to EcNR2.nuc5- ($54.3 \pm 5.6\%$)
504 (Figure 5B).

505 Given the higher single-cycle conversion rate of EcNR2.nuc5- compared to BioDesignER (Figure 2C,
506 right panel), we were surprised by the comparable performance of the two strains over multiple
507 recombineering cycles. We partly attribute this parity to uncharacteristically low and sporadic single-
508 cycle efficiencies that we repeatedly observed for EcNR2.nuc5- replicates (Supplementary Figure S7).
509 Regardless, while both BioDesignER and EcNR2.nuc5- exhibited similar multiplex editing efficiencies,
510 EcNR2.nuc5- requires culturing at 30-32°C and is a persistent mutator, which increases recombineering
511 cycle time and basal mutation rate, respectively - thus limiting its overall utility as a reliable strain for
512 multiplex genome editing.

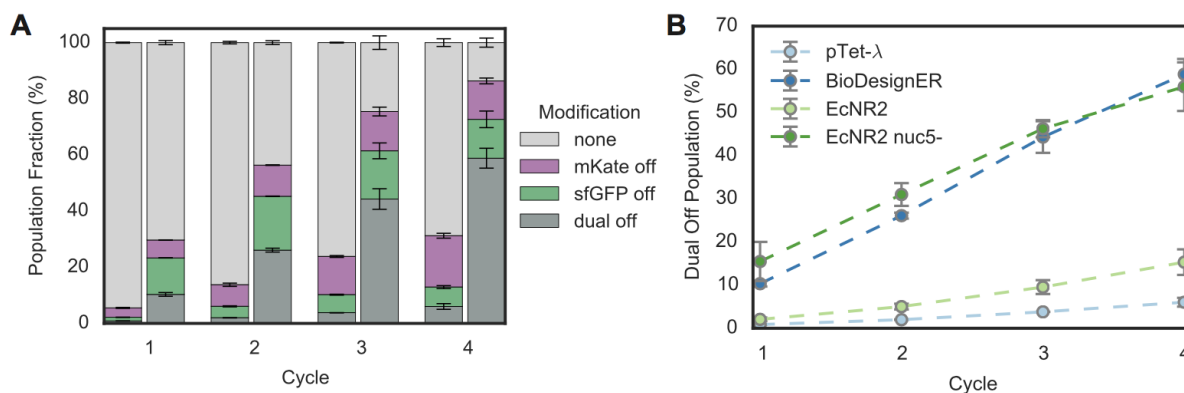


Figure 5. Multi-Cycle Recombineering (A) The fraction of each genotype (i.e. modification type) was measured via flow cytometry for pTet-λ (left) and BioDesignER (right) after each cycle of recombineering. Errors bars represent ± 1 standard deviation. (B) The fraction of each strain population in which both markers were edited (dual off genotype) is shown across all four recombineering cycles. Errors bars represent ± 1 standard deviation.

513

514 DISCUSSION

515 High-efficiency genome engineering in bacteria enables breadth (24) and depth (17) explorations of
516 genotypic diversity to enhance engineered behaviors. However, to date, no platform strain exists that
517 incorporates a suite of core functions to provide efficient recombineering and regulate both genome
518 engineering functions and cellular programs. BioDesignER is a high recombineering fidelity
519 recombineering strain constructed to rapidly explore and optimize engineered functions. It incorporates
520 many genomic modifications that increase recombination efficiency and reduce cycle time for
521 recombineering workflows while minimizing off-target mutations. BioDesignER includes four
522 independent inducible regulators to control recombineering and accommodate additional user designs.
523 We have characterized eight Safe Site integration loci distributed across the genome and found that
524 seven enable reliable gene expression and mutagenesis.

525
526 BioDesignER enables rapid selection-based recombineering workflows with no requirements for
527 plasmid transformation or curing. Reliable engineering of sequential genome integrations with
528 established recombineering approaches, such as the use of plasmids pSIM5 (12) or pKD20 (10), require
529 transformation and curing procedures of plasmid-encoded recombineering functions for each
530 integration stage. These requirements increase the time required for individual genome editing steps
531 by multiple days. Anecdotally, we have found plasmid-based recombineering systems unreliable for
532 conducting multiple editing cycles from a single transformation of the recombineering plasmid. We
533 speculate that the failure to achieve multi-cycle genome editing from plasmid-based recombineering
534 solutions may be related to the accumulation of mutations spurred by maintenance or leaky expression
535 of λ -Red genes over many generations. In contrast, we have completed all of the scar-free DNA
536 recombineering workflows reported here with no restoration or replacement of the minimized pTet λ -
537 Red cassette.

538
539 We have increased recombineering fidelity in BioDesignER by striking a balance between
540 recombination efficiency and mutagenesis rates. A high recombineering fidelity platform such as this
541 may provide new avenues to multiplex genome remodeling using CRISPR-Cas9 techniques. CRISPR-
542 Cas9 genome editing approaches in bacteria are limited by recombination efficiency to rescue double-
543 strand breaks. Linking CRISPR-Cas9 counterselection of native sequences with high-efficiency, multi-
544 site recombineering may allow concurrent selection of many modifications from a large bacterial
545 population with little off-target activity, thereby enabling researchers to explore unprecedented genetic
546 diversity.

547
548 While BioDesignER exhibits robust functionalities with respect to recombineering fidelity, comparing the
549 recombination efficiency of the BioDesignER lineage to EcNR2-derived strains reveals inconsistent
550 results related to culture temperatures. Specifically, we found a nearly two-fold reduction in
551 recombination efficiency for BioDesignER at 30°C compared to 37°C, resulting in recombineering
552 efficiencies similar to EcNR2 (Figure 2C). This reduction suggests some uncharacterized temperature-
553 specific reduction in recombination efficiency and could reflect reduced ssDNA access to the replication
554 fork, lower ssDNA half-life at reduced temperatures, or perhaps uncharacterized temperature-
555 dependent expression of the λ -Red machinery from pTet.

556
557 While constructing BioDesignER, we developed multiple selection/counter-selection strategies that may
558 be of general use for bacterial genome engineering. These strategies combine selection/counter-
559 selection and fluorescence screening components to accelerate scar-free genome engineering.
560 Specifically, the genetic cassettes utilize selection/counter-selection of *thyA*, building on work from
561 FRUIT (48). This approach requires two recombineering transformations: a dsDNA integration of the
562 fluorescence-coupled *thyA* cassette at the target genomic locus followed by removal of the cassette
563 using ssDNA or dsDNA. The genetic modification of interest can be incorporated at either integration
564 stage. In comparison, CRISPR-based genome editing workflows, which are gaining popularity, require

565 multiple steps including guide plasmid construction, co-transformation with Cas9, and subsequent
566 curing. Thus, the selection/counter selection methodologies developed here allow a simple and
567 effective approach to genome engineering.

568

569 Development of BioDesignER points to genome design strategies for next-generation biotechnology
570 hosts. As synthetic biology matures, the application space is expanding beyond prototypical genetic
571 circuits and metabolic pathways in laboratory environments to robust engineered functions in ecologies
572 with high biotic and abiotic complexity, including soil, wastewater, and the human gut (49). Efficient and
573 sustained activity of engineered functions in these environments will require programmed behaviors to
574 be optimized in phylogenetically diverse microbes. We anticipate the integrative approach used to
575 develop and characterize BioDesignER can be used as a template to develop high-efficiency
576 recombineering platforms for new bacterial hosts.

577

578 **ACKNOWLEDGEMENTS**

579 The authors would like to thank Vivek Mutalik for providing the *cymR* expression construct and the core
580 promoter sequence used to design the Tet-based λ-Red expression system. We would also like to thank
581 the Li Ka Shing Flow Cytometry Facility at UC Berkeley.

582 **FUNDING**

583 This work was supported by the Department of Energy Genome Science program within the Office of
584 Biological and Environmental Research [grant number DE-SC008812, Funding Opportunity
585 Announcement DE-FOA-0000640]. H.S.R is supported by a National Science Foundation (NSF)
586 Graduate Research Fellowship and a National Institutes of Health (NIH) Genomics and Computational
587 Biology Training Program [5T32HG000047-18]. Funding for open access charge: DE-SC008812.

588 *Conflict of interest statement.* None declared.

589 **REFERENCES**

- 590 1. Khalil,A.S. and Collins,J.J. (2010) Synthetic biology: applications come of age. *Nat Rev Genet*, **11**,
591 367–379.
- 592 2. Weber,W. and Fussenegger,M. (2011) Emerging biomedical applications of synthetic biology. *Nat
593 Rev Genet*, **13**, 21–35.
- 594 3. Tyo,K.E.J., Ajikumar,P.K. and Stephanopoulos,G. (2009) Stabilized gene duplication enables long-
595 term selection-free heterologous pathway expression. *Nat Biotechnol*, **27**, 760–765.
- 596 4. Friehs,K. (2004) Plasmid copy number and plasmid stability. *Adv Biochem Eng Biotechnol*, **86**, 47–
597 82.
- 598 5. Bassalo,M.C., Garst,A.D., Halweg-Edwards,A.L., Grau,W.C., Domaille,D.W., Mutalik,V.K.,
599 Arkin,A.P. and Gill,R.T. (2016) Rapid and Efficient One-Step Metabolic Pathway Integration in
600 *E. coli*. *ACS Synth. Biol.*, **5**, 561–568.
- 601 6. Lee,J.W., Gyorgy,A., Cameron,D.E., Pyenson,N., Choi,K.R., Way,J.C., Silver,P.A., Del Vecchio,D.

602 and Collins,J.J. (2016) Creating Single-Copy Genetic Circuits. *Molecular Cell*, **63**, 329–336.

603 7. Esvelt,K.M. and Wang,H.H. (2013) Genome-scale engineering for systems and synthetic biology.
604 *Molecular Systems Biology*, **9**, 641–641.

605 8. Bryant,J.A., Sellars,L.E., Busby,S.J.W. and Lee,D.J. (2014) Chromosome position effects on gene
606 expression in Escherichia coli K-12. *Nucleic Acids Res*, **42**, 11383–11392.

607 9. Murphy,K.C. (1998) Use of bacteriophage lambda recombination functions to promote gene
608 replacement in Escherichia coli. *J. Bacteriol.*, **180**, 2063–2071.

609 10. Datsenko,K.A. and Wanner,B.L. (2000) One-step inactivation of chromosomal genes in
610 Escherichia coli K-12 using PCR products. *Proc Natl Acad Sci USA*, **97**, 6640–6645.

611 11. Ellis,H.M., Yu,D., DiTizio,T. and Court,D.L. (2001) High efficiency mutagenesis, repair, and
612 engineering of chromosomal DNA using single-stranded oligonucleotides. *Proc Natl Acad Sci
613 USA*, **98**, 6742–6746.

614 12. Datta,S., Costantino,N. and Court,D.L. (2006) A set of recombineering plasmids for gram-negative
615 bacteria. *Gene*, **379**, 109–115.

616 13. Sharan,S.K., Thomason,L.C., Kuznetsov,S.G. and Court,D.L. (2009) Recombineering: a
617 homologous recombination-based method of genetic engineering. *Nature Protocols*, **4**, 206–223.

618 14. Baba,T., Ara,T., Hasegawa,M., Takai,Y., Okumura,Y., Baba,M., Datsenko,K.A., Tomita,M.,
619 Wanner,B.L. and Mori,H. (2006) Construction of Escherichia coli K-12 in-frame, single-gene
620 knockout mutants: the Keio collection. *Molecular Systems Biology*, **2**, 1–11.

621 15. Warner,J.R., Reeder,P.J., Karimpour-Fard,A., Woodruff,L.B.A. and Gill,R.T. (2010) Rapid profiling
622 of a microbial genome using mixtures of barcoded oligonucleotides. *Nat Biotechnol*, **28**, 856–862.

623 16. Freed,E.F., Winkler,J.D., Weiss,S.J., Garst,A.D., Mutualik,V.K., Arkin,A.P., Knight,R. and Gill,R.T.
624 (2015) Genome-Wide Tuning of Protein Expression Levels to Rapidly Engineer Microbial Traits.
625 *ACS Synth. Biol.*, **4**, 1244–1253.

626 17. Garst,A.D., Bassalo,M.C., Pines,G., Lynch,S.A., Halweg-Edwards,A.L., Liu,R., Liang,L., Wang,Z.,
627 Zeitoun,R., Alexander,W.G., *et al.* (2016) Genome-wide mapping of mutations at single-
628 nucleotide resolution for protein, metabolic and genome engineering. *Nat Biotechnol*, **35**, 1–12.

629 18. Wang,H.H., Isaacs,F.J., Carr,P.A., Sun,Z.Z., Xu,G., Forest,C.R. and Church,G.M. (2009)
630 Programming cells by multiplex genome engineering and accelerated evolution. *Nature*, **460**,
631 894–898.

632 19. Isaacs,F.J., Carr,P.A., Wang,H.H. and Lajoie,M.J. (2011) Precise manipulation of chromosomes in
633 vivo enables genome-wide codon replacement. *Science*, 10.1126/science.1204763.

634 20. Lajoie,M.J., Rovner,A.J., Goodman,D.B., Aerni,H.-R., Haimovich,A.D., Kuznetsov,G., Mercer,J.A.,
635 Wang,H.H., Carr,P.A., Mosberg,J.A., *et al.* (2013) Genomically recoded organisms expand
636 biological functions. *Science*, **342**, 357–360.

637 21. Lajoie,M.J., Kosuri,S., Mosberg,J.A., Gregg,C.J., Zhang,D. and Church,G.M. (2013) Probing the
638 limits of genetic recoding in essential genes. *Science*, **342**, 361–363.

639 22. Wang,H.H., Kim,H., Cong,L., Jeong,J. and Bang,D. (2012) Genome-scale promoter engineering
640 by coselection MAGE. *Nature*, 10.1038/nmeth.1971.

641 23. Wang,H.H., Huang,P.-Y., Xu,G., Haas,W., Marblestone,A., Li,J., Gygi,S.P., Forster,A.C.,
642 Jewett,M.C. and Church,G.M. (2012) Multiplexed in vivo His-tagging of enzyme pathways for in
643 vitro single-pot multienzyme catalysis. *ACS Synth. Biol.*, **1**, 43–52.

644 24. Zeitoun,R.I., Garst,A.D., Degen,G.D., Pines,G., Mansell,T.J., Glebes,T.Y., Boyle,N.R. and
645 Gill,R.T. (2015) Multiplexed tracking of combinatorial genomic mutations in engineered cell
646 populations. *Nat Biotechnol*, **33**, 1–10.

647 25. Zeitoun,R.I., Pines,G., Grau,W.C. and Gill,R.T. (2017) Quantitative Tracking of Combinatorially
648 Engineered Populations with Multiplexed Binary Assemblies. *ACS Synth. Biol.*, **6**, 619–627.

649 26. Glickman,B.W. and Radman,M. (1980) Escherichia coli mutator mutants deficient in methylation-
650 instructed DNA mismatch correction. *Proc Natl Acad Sci USA*, **77**, 1063–1067.

651 27. Schaaper,R.M. and Dunn,R.L. (1987) Spectra of spontaneous mutations in Escherichia coli
652 strains defective in mismatch correction: the nature of in vivo DNA replication errors. *Proc Natl
653 Acad Sci USA*, **84**, 6220–6224.

654 28. Sawitzke,J.A., Thomason,L.C., Costantino,N., Bubunenko,M., Datta,S. and Court,D.L. (2007)
655 Recombineering: in vivo genetic engineering in *E. coli*, *S. enterica*, and beyond. *Meth. Enzymol.*,
656 **421**, 171–199.

657 29. Wang,H.H., Xu,G., Vonner,A.J. and Church,G. (2011) Modified bases enable high-efficiency
658 oligonucleotide-mediated allelic replacement via mismatch repair evasion. *Nucleic Acids Res*, **39**,
659 7336–7347.

660 30. Nyerges,Á., Csörgő,B., Nagy,I., Latinovics,D., Szamecz,B., Pósfaí,G. and Pál,C. (2014)
661 Conditional DNA repair mutants enable highly precise genome engineering. *Nucleic Acids Res*,
662 **42**, e62–e62.

663 31. Lennen,R.M., Nilsson Wallin,A.I., Pedersen,M., Bonde,M., Luo,H., Herrgård,M.J. and
664 Sommer,M.O.A. (2016) Transient overexpression of DNA adenine methylase enables efficient
665 and mobile genome engineering with reduced off-target effects. *Nucleic Acids Res*, **44**, e36–e36.

666 32. Sarkar,S., Ma,W.T. and Sandri,G.H. (1992) On fluctuation analysis: a new, simple and efficient
667 method for computing the expected number of mutants. *Genetica*, **85**, 173–179.

668 33. Ma,W.T., Sandri,G.H. and Sarkar,S. (1992) Analysis of the Luria–Delbrück distribution using
669 discrete convolution powers. *Journal of Applied Probability*.

670 34. Sergueev,K., Yu,D., Austin,S. and Court,D. (2001) Cell toxicity caused by products of the p(L)
671 operon of bacteriophage lambda. *Gene*, **272**, 227–235.

672 35. Lawther,R.P., Calhoun,D.H., Adams,C.W., Hauser,C.A., Gray,J. and Hatfield,G.W. (1981)
673 Molecular basis of valine resistance in Escherichia coli K-12. *Proc Natl Acad Sci USA*, **78**, 922–
674 925.

675 36. Lawther,R.P., Calhoun,D.H., Gray,J., Adams,C.W., Hauser,C.A. and Hatfield,G.W. (1982) DNA
676 sequence fine-structure analysis of ilvG (IlvG+) mutations of Escherichia coli K-12. *J. Bacteriol.*,
677 **149**, 294–298.

678 37. Tedin,K. and Norel,F. (2001) Comparison of Δ relA strains of Escherichia coli and *Salmonella*
679 enterica serovar Typhimurium suggests a role for ppGpp in attenuation regulation of branched-
680 chain *J. Bacteriol.*, 10.1128/JB.183.21.6184–6196.2001.

681 38. Lajoie,M.J., Gregg,C.J., Mosberg,J.A., Washington,G.C. and Church,G.M. (2012) Manipulating
682 replisome dynamics to enhance lambda Red-mediated multiplex genome engineering. *Nucleic
683 Acids Res*, **40**, e170–e170.

684 39. Mosberg,J.A., Gregg,C.J., Lajoie,M.J., Wang,H.H. and Church,G.M. (2012) Improving lambda red
685 genome engineering in Escherichia coli via rational removal of endogenous nucleases. *PLoS
686 ONE*, **7**, e44638.

687 40. Glascock,C.B. and Weickert,M.J. (1998) Using chromosomal lacIQ1 to control expression of
688 genes on high-copy-number plasmids in *Escherichia coli*. *Gene*, **223**, 221–231.

689 41. Choi,Y.J., Morel,L., Le François,T., Bourque,D., Bourget,L., Groleau,D., Massie,B. and
690 Míguez,C.B. (2010) Novel, versatile, and tightly regulated expression system for *Escherichia coli*
691 strains. *Appl. Environ. Microbiol.*, **76**, 5058–5066.

692 42. Khlebnikov,A., Skaug,T. and Keasling,J.D. (2002) Modulation of gene expression from the
693 arabinose-inducible araBAD promoter. *J Ind Microbiol Biotechnol*, **29**, 34–37.

694 43. Price,M.N., Wetmore,K.M., Waters,R.J., Callaghan,M., Ray,J., Liu,H., Kuehl,J.V., Melnyk,R.A.,
695 Lamson,J.S., Suh,Y., *et al.* (2018) Mutant phenotypes for thousands of bacterial genes of
696 unknown function. *Nature*, **557**, 503–509.

697 44. Gama-Castro,S., Salgado,H., Santos-Zavaleta,A., Ledezma-Tejeida,D., Muñiz-Rascado,L.,
698 García-Sotelo,J.S., Alquicira-Hernández,K., Martínez-Flores,I., Pannier,L., Castro-
699 Mondragón,J.A., *et al.* (2016) RegulonDB version 9.0: high-level integration of gene regulation,
700 coexpression, motif clustering and beyond. *Nucleic Acids Res*, **44**, D133–43.

701 45. Bipatnath,M., Dennis,P.P. and Bremer,H. (1998) Initiation and velocity of chromosome replication
702 in *Escherichia coli* B/r and K-12. *J. Bacteriol.*, **180**, 265–273.

703 46. Reynolds,T.S. and Gill,R.T. (2015) Quantifying Impact of Chromosome Copy Number on
704 Recombination in *Escherichia coli*. *ACS Synth. Biol.*, **4**, 776–780.

705 47. Lee,H., Popodi,E., Tang,H. and Foster,P.L. (2012) Rate and molecular spectrum of spontaneous
706 mutations in the bacterium *Escherichia coli* as determined by whole-genome sequencing. *Proc.*
707 *Natl. Acad. Sci. U.S.A.*, **109**, E2774–83.

708 48. Stringer,A.M., Singh,N., Yermakova,A., Petrone,B.L., Amarasinghe,J.J., Reyes-Diaz,L.,
709 Mantis,N.J. and Wade,J.T. (2012) FRUIT, a scar-free system for targeted chromosomal
710 mutagenesis, epitope tagging, and promoter replacement in *Escherichia coli* and *Salmonella*
711 *enterica*. *PLoS ONE*, **7**, e44841.

712 49. Venturelli,O.S., Egbert,R.G. and Arkin,A.P. (2016) Towards Engineering Biological Systems in a
713 Broader Context. *J. Mol. Biol.*, **428**, 928–944.

714